

## **SUPPLEMENTARY MATERIALS**

### **Microporous Polymer Modified Glassy Carbon Electrodes for Electrochemical Detection of Metronidazole: Experimental and Theoretical Insights**

**Héctor Quiroz-Arturo<sup>1</sup>, Carlos Reinoso<sup>2</sup>, Ullrich Scherf<sup>3,\*</sup>, and Alex Palma-Cando<sup>1,\*</sup>**

<sup>1</sup> Grupo de Investigación Aplicada en Materiales y Procesos (GIAMP), School of Chemical Sciences and Engineering, Yachay Tech University, Hda. San José s/n y Proyecto Yachay, 100115 Urcuqui, Ecuador

<sup>2</sup> School of Physical Sciences and Nanotechnology, Yachay Tech University, Hda. San José s/n y Proyecto Yachay, 100115 Urcuqui, Ecuador

<sup>3</sup> Department of Chemistry, Macromolecular Chemistry and Wuppertal Center for Smart Materials @ Systems (CM@S), Bergische Universität Wuppertal, Gaußstr. 20, 42119 Wuppertal, Germany

\* Correspondence: scherf@uni-wuppertal.de (U. S.); apalma@yachaytech.edu.ec (A. P.-C.)

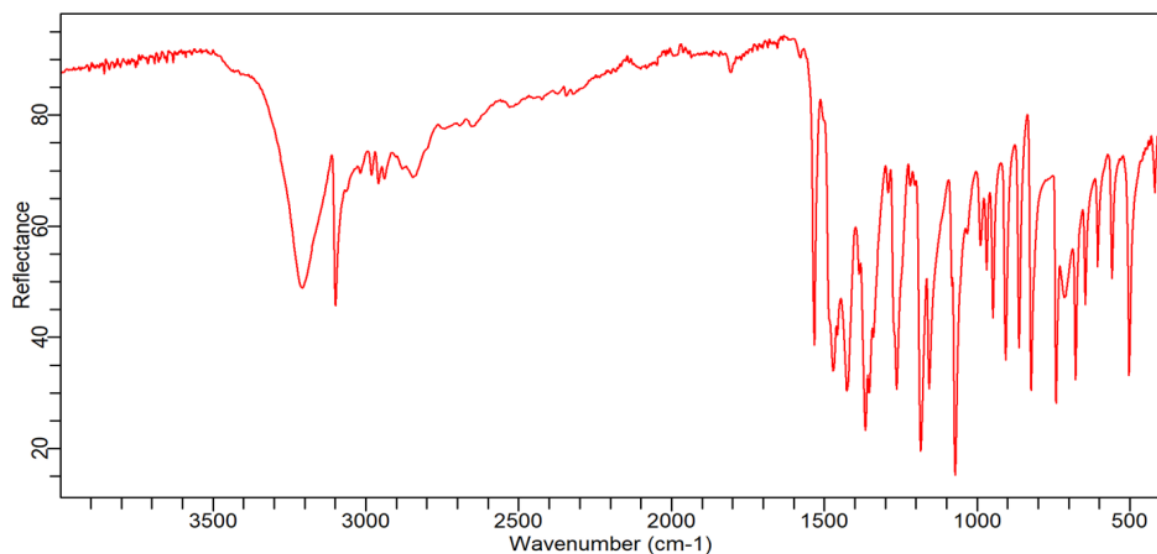


**Figure S1.** FT-IR spectrum of purified metronidazole. The  $1263.57\text{ cm}^{-1}$  and  $1185.29\text{ cm}^{-1}$  peaks correspond to the bonds  $-\text{C}=\text{C}-$  and  $-\text{C}=\text{N}-$  of the imidazole cycle. The broad absorption band at  $3211.10\text{ cm}^{-1}$  and the peak at  $3099.28\text{ cm}^{-1}$  indicate the presence of hydroxyl group. Absorption bands at  $1533.8\text{ cm}^{-1}$  and  $1366.07\text{ cm}^{-1}$  correspond to the stretching vibrations of the  $\text{NO}_2$  group [S1,S2].

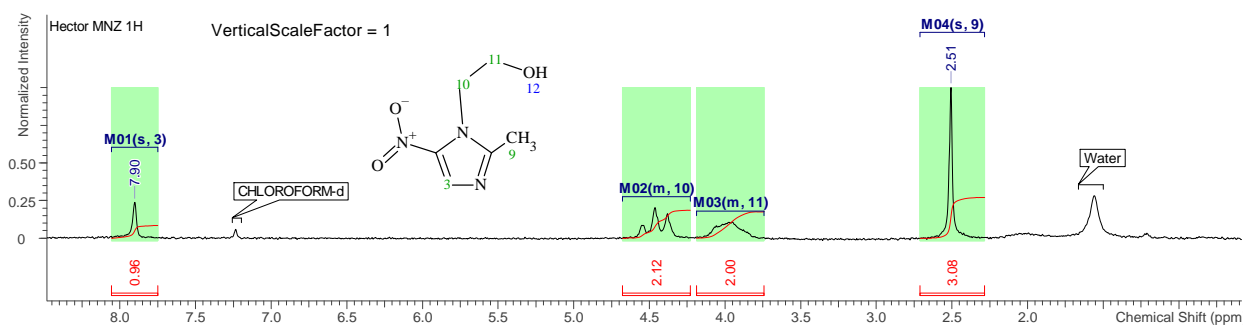


**Figure S2.** NMR spectrum for purified metronidazole.  $^1\text{H}$  NMR ( $60\text{ MHz}$ , CHLOROFORM-d)  $\delta$  ppm 2.51 (s, 3 H) 3.74 - 4.19 (m, 2 H) 4.23 - 4.68 (m, 2 H) 7.90 (s, 1 H). No hydroxyl proton signal was identified [S3].

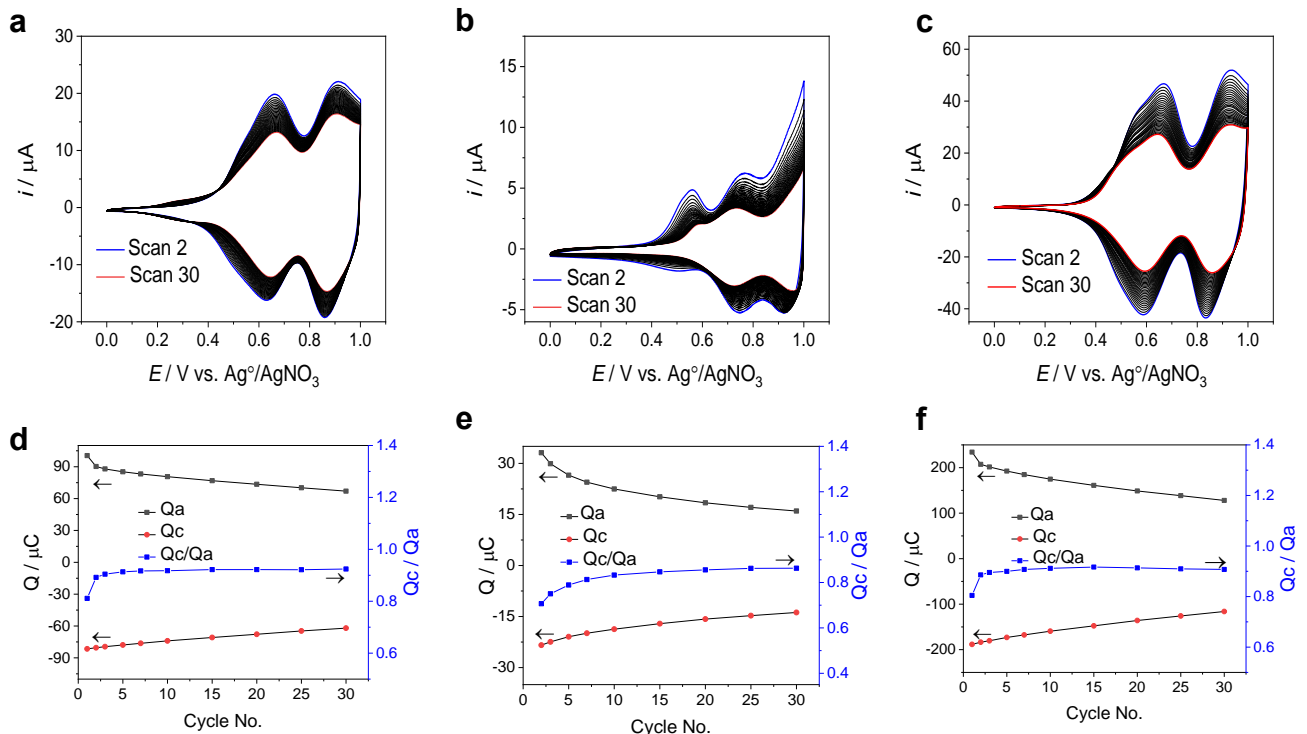


**Figure S3.** Electrochemical stability of (a) PCBP, (b) PTCB, and (c) PTPTCzSiOH films on GCE obtained in a free monomer solution, ACN/TBAP 0.1 M. The applied potential range was 0 – 1.0 V with a sweeping rate of 0.1 V/s. The variation of the anodic and cathodic charge ( $Q_a$  and  $Q_c$ , left axis) and the  $Q_c/Q_a$  (right axis, blue curve) during the 30 cycles for (d) PCBP, (e) PTCB, and (f) PTPTCzSiOH films on GCE are also shown.

**Table S1.** Electrochemical stability and reversibility of polymer films in ACN/TBAP 0.1M represented as the percentage of cathodic current loss between the second and thirtieth cycle (% $Q_c$ ), and cathodic to anodic charge ratio at the thirtieth cycle ( $Q_c/Q_a$ ), respectively.

Polymer	% $Q_c$	$Q_c/Q_a$
PCBP	23.0	0.92
PTCB	40.9	0.86
PTPTCzSiOH	36.7	0.91

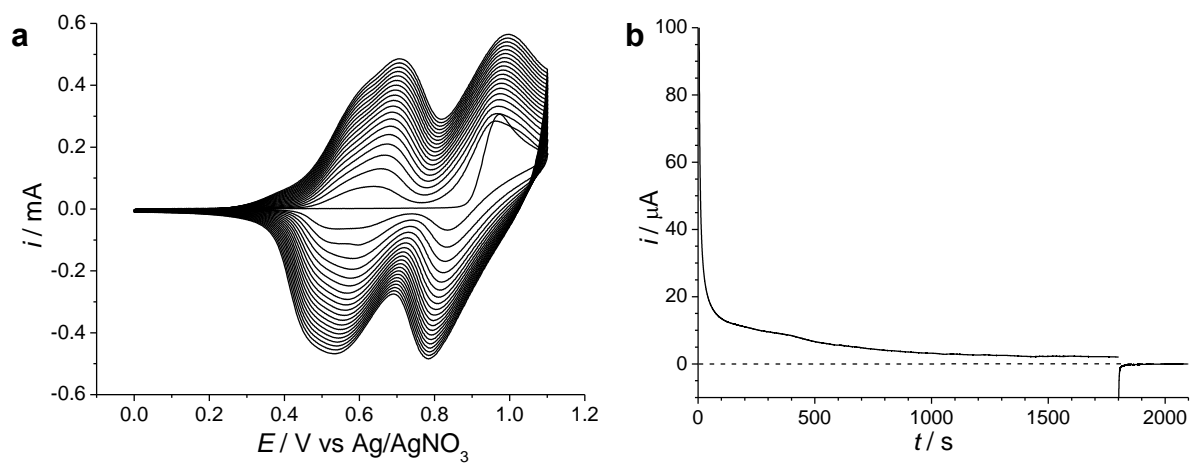


**Figure S4.** (a) Electropolymerization of TPTCzSiOH film on ITO scanning from 0 V vs.  $\text{Ag}/\text{AgNO}_3$  to 1.1 V for 20 cycles at 0.1 Vs-1 in a 0.1 M TBAP/ACN solution with 0.1 mM monomer concentration. (b) Chronoamperograms for thin ITO-PTPTCzSiOH films with an oxidative potential applied of 1 V for 30 min followed by a dedoping potential of 0 V for 5 min.

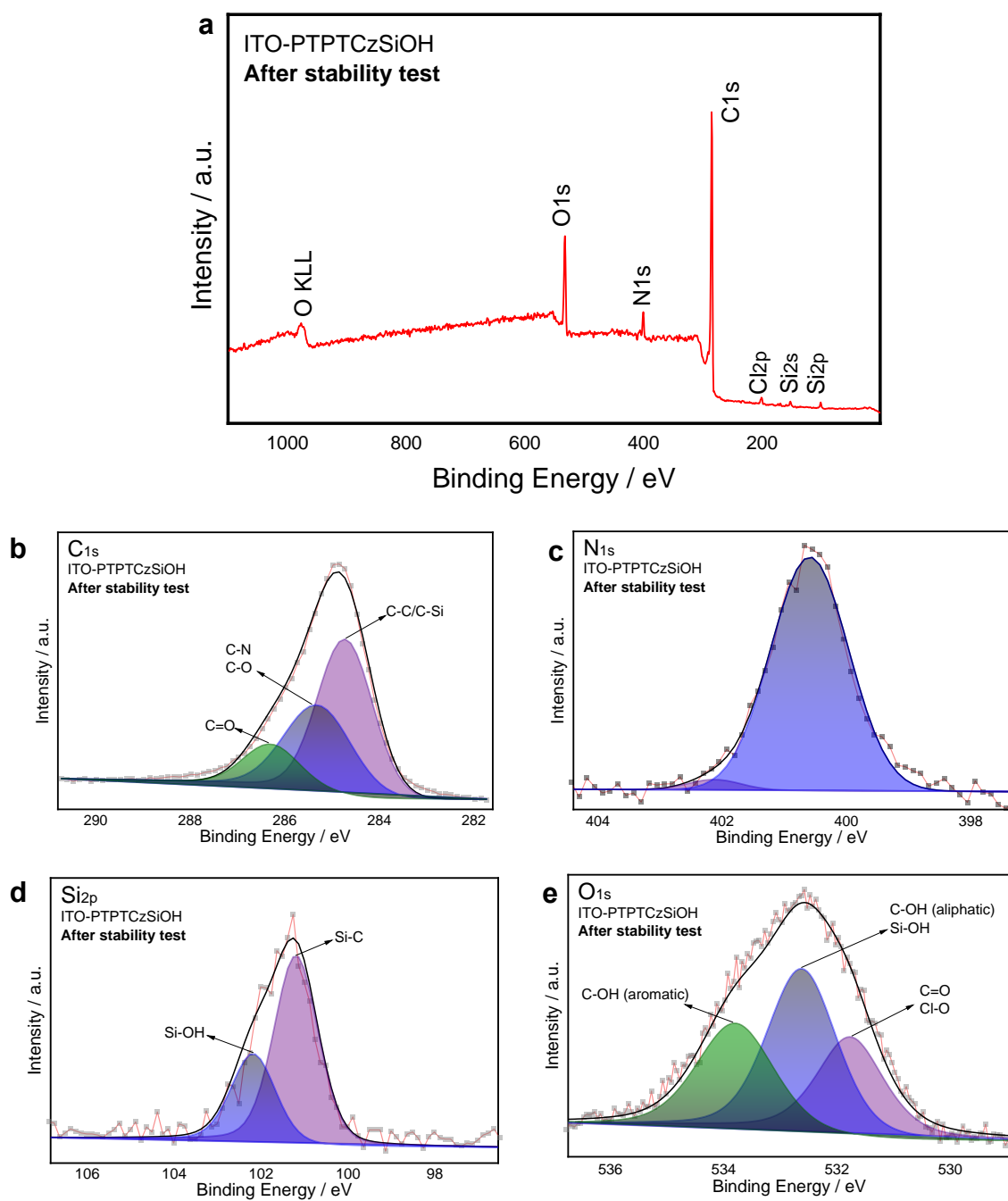


**Figure S5.** XPS spectra of the (a) survey scan, and high-resolution spectra of (b) C1s, (c) N1s, (d) Si2p, and (e) O1s of ITO-PTPTCzSiOH electrode after the oxidative treatment described in Figure S4.

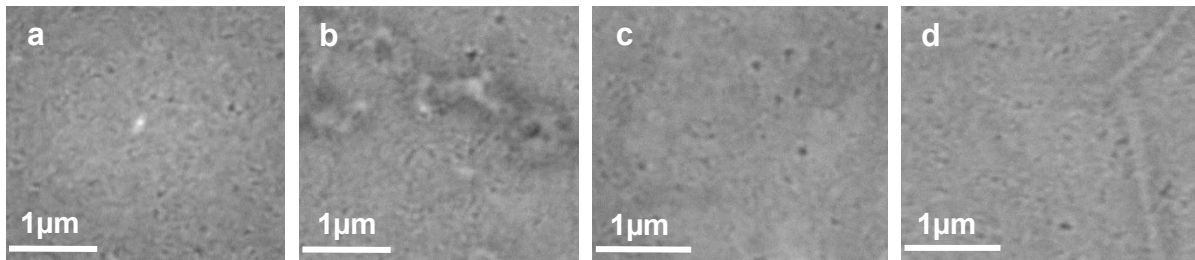


**Figure S6.** The top-view SEM topographies of (a) bare ITO, (b) PCBP-ITO, (c) PTCB-ITO, and (d) PTPTCzSiOH-ITO electrodes.

**Table S2.** Current response for the cathodic reduction peak in the electrochemical detection of 50  $\mu$ M MNZ. The current ratios of the peak between MPN-modified and non-modified GC electrodes are also listed.

Electrode	$E_p$ (V)	$i_p$ ( $\mu$ A)	$i_p / i_{p\text{ GC}}$
GC	-0.60	-6.60	1.0
GC-PCBP	-0.89	-13.0	1.9
GC-PTCB	-0.66	-22.6	3.4
GC-PTPTCzSiOH	-0.88	-23.9	3.6

**Table S3.** Experimental and theoretical values of the onset oxidation potential ( $E_{onset}$ ) and the energy of HOMO orbital ( $E_{HOMO}$ ).

Monomer	$E_{onset}$ (V)	$E_{HOMO}$ (eV) experimental	$E_{HOMO}$ (eV) theoretical
CBP	0.86	-5.96	-5.57
TCB	1.00	-6.10	-5.72
TPTCzSiOH	0.85	-5.95	-5.62

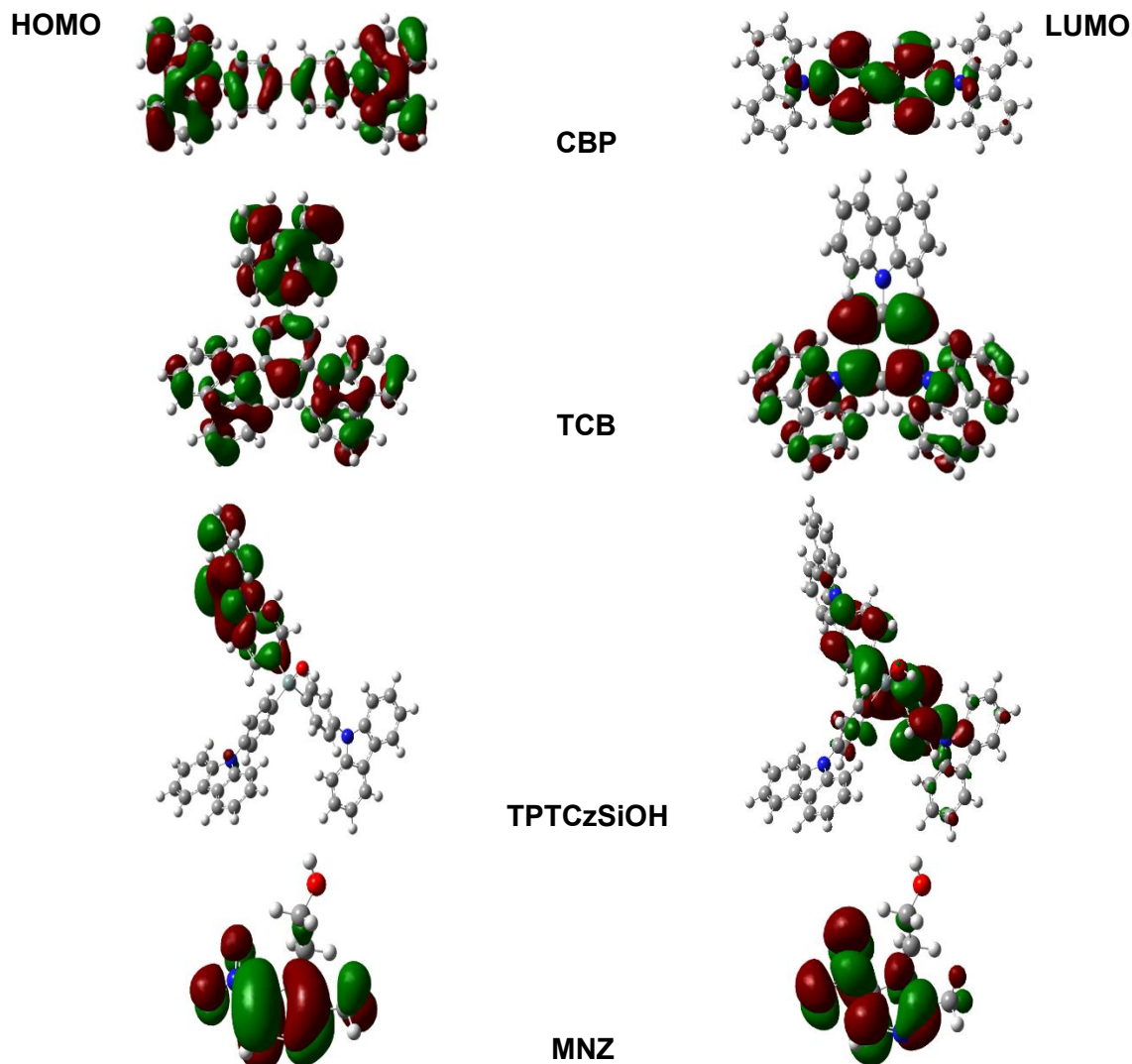


**Figure S7.** The contour representation of frontier molecular orbitals computed by DFT/B3LYP method for investigated molecules.

## References

- S1. Myhal, A. V.; Golovchenko, O.S.; Krutskikh, T. V.; Gubar, S.M.; Georgiyants, V.A. IR-Spectroscopy Research into the Structure of Products of Interaction between Metronidazole and Metal Salts. *Der Pharma Chemica* **2016**, 8, 148–154.
- S2. Szente, V.; Baska, F.; Zelkó, R.; Süvegh, K. Prediction of the Drug Release Stability of Different Polymeric Matrix Tablets Containing Metronidazole. *Journal of Pharmaceutical and Biomedical Analysis* **2011**, 54, 730–734, doi:10.1016/j.jpba.2010.11.005.
- S3. Kalinowska-Lis, U.; Felczak, A.; Checińska, L.; Zawadzka, K.; Patyna, E.; Lisowska, K.; Ochocki, J. Synthesis, Characterization and Antimicrobial Activity of Water-Soluble Silver(I) Complexes of Metronidazole Drug and Selected Counter-Ions. *Dalton Transactions* **2015**, 44, 8178–8189, doi:10.1039/c5dt00403a.